

Thick accretion disk configurations around a compact object in the brane-world scenario

Yunzhu Wei¹, Songbai Chen^{1,2*}, Jiliang Jing^{1,2 †}

¹*Department of Physics, Key Laboratory of Low Dimensional Quantum Structures and Quantum Control of Ministry of Education, Institute of Interdisciplinary Studies, Synergetic Innovation Center for Quantum Effects and Applications, Hunan Normal University, Changsha, Hunan 410081, People's Republic of China*

²*Center for Gravitation and Cosmology, College of Physical Science and Technology, Yangzhou University, Yangzhou 225009, People's Republic of China*

Abstract

We have studied equipotential surfaces of a thick accretion disk around a Casadio-Fabbri-Mazzacurati (CFM) compact object in the brane-world scenario, which owns a mass parameter together with a parameterized post-newtonian (PPN) parameter. With the increase of the PPN parameter, the size of the thick accretion disk decreases, but the corresponding Roche lobe size increases. Thus, the larger PPN parameter yields the larger region of existing bound disk structures where the fluid is not accreted into the central wormhole. Moreover, with the increase of the PPN parameter, the position of the Roche lobe gradually moves away from the central compact object, the thickness of the region enclosed by the Roche lobe decreases near the compact object, but increases in the region far from the compact object. Our results also show that the pressure gradient in the disk decreases with the PPN parameter. These effects of the PPN parameter on thick accretion disk could help to further understand compact objects in brane-world scenario.

PACS numbers: 04.70.-s, 98.62.Mw, 97.60.Lf

* Corresponding author: csb3752@hunnu.edu.cn

† jljing@hunnu.edu.cn

I. INTRODUCTION

A compact object at the center of galaxy should own an accretion disk in which matter flows spiral into the central celestial body together with dropping off their initial angular momentums outwards as well as releasing their gravitational potential energy into heat. The analyses of the properties of accretion disks can disclose the motion of matter near the central celestial body, which could offer the opportunity to capture some information from the celestial body because the accretion occurs in the strong gravity region. Therefore, the studies of accretion disks have contributed to examining the predictions from various theories of gravity including general relativity, which may deepen the understanding of the gravitational interaction [1–19]. Generally, in term of their geometrical thickness, the accretion disk models can be classified into two types. One of them is the so-called geometrically thin model in which the disk height is much smaller than the characteristic radius of the disk [1–3]. The heat generated by stress and dynamic friction in the disk can be effectively dispersed through the radiation over its surface, which leads to that the disk is cool. The other type is the geometrically thick model [4–10] in which the energy conversion into radiation is inefficient and the temperature of the accretion gas is higher than that in the previous thin disk model. It is widely believed that there exist thick accretion disks in the vicinity of many X-ray binaries and active galactic nuclei.

In the real astrophysical systems, the matter accretion is a highly complicated dynamic process and its complete description must resort to the high precise numerical calculations, such as general relativistic magnetohydrodynamics (GRMHD) simulations. However, in the past few decades, a simple and analytical model of geometrically thick and stationary tori orbiting black holes, known as Polish doughnuts [10], has been attracted a lot of attention. Although the matter in this model is assumed to be in equilibrium and is not actually accreted by the black hole, the configurations of these geometrically thick equilibrium tori carry a lot of important characteristic information on the spacetime in the strong field regions. Moreover, due to the fluid being in equilibrium, Polish doughnuts are often used as an initial condition for numerical simulations of accretion flows. Thus, the equilibrium tori around black holes have been studied in spacetimes in general relativity and in other alternative theories of gravity (for a review see e.g. [11–13]). Recently, thick accretion disks have been investigated in the background of the spherically symmetric black hole in Born-Infeld teleparallel gravity [20] and probe effects of the teleparallel parameter on the equilibrium tori around the black hole, which show that the size of the disk monotonically decreases with the teleparallel parameter [21]. The non-selfgravitating equilibrium tori have also been studied in the background of the parameterised Rezzolla-

Zhidenko black hole [22]. It is found that there exist standard “single-torus” and non-standard “double-tori” solutions within the allowed space of parameters, which means that the parameterised Rezzolla-Zhidenko black hole owns a much richer class of equilibrium tori. Moreover, the magnetized accretion disks around Kerr black holes with scalar hair have been respectively studied with the constant angular momentum [23] and the nonconstant angular momentum [24], which could help further constrain the no-hair hypothesis by combining with future observations. The stationarily and geometrically thick tori with the constant angular momentum are researched in the background of a nonrotating black hole in $f(R)$ -gravity with a Yukawa-like modification to the Newtonian potential[25]. Making a comparison with the Kerr black hole in the general relativity, it is easy to find that there are notable changes in the configurations of the disks. Moreover, the equilibrium solutions of magnetised, geometrically thick accretion disks are also studied with the nonconstant specific angular momentum distribution in the Kerr black hole spacetime [26].

We here focus on thick accretion disk configurations around a compact object in the brane-world theory. According to the brane-world scenario [27, 28], the usual four-dimensional spacetime might be a three-brane embedded in a five-dimensional spacetime (the bulk). All of matter fields including electromagnetic field are confined to the three brane, and only gravity can freely propagate both in brane and bulk. High energy corrections and Weyl stresses from bulk gravitons mean that a static black hole solution on the brane is no longer the Schwarzschild solution [29]. However, the Einstein field equations in five dimensions are found to admit more spherically symmetric solutions on the brane than in four-dimensional general relativity. The first black hole solution on the brane obtained in [29], has the same form as the usual Reissner-Nordström solution, in which a tidal Weyl parameter plays the role of the electric charge. The star solution with a constant density interior has been studied on the brane [30]. The black hole solutions in the brane-world model and the corresponding observable effects have also been widely studied [31–40]. The properties of a thin accretion disks around a brane world black hole have been investigated [41], and it is shown that the particular signatures appeared in the electromagnetic spectrum could offer a the possibility to directly test physical models with extra dimension by using astrophysical observations from accretion disks. We here will consider a spherically symmetric solution in the brane world obtained by Casadio, Fabbri and Mazzacurati [42]. The properties of a thin accretion disks around the CFM compact object have also been studied in [41]. However, the thick accretion disk configurations around the CFM compact object remain open. The main purpose of this paper is to probe the properties of thick accretion disk configurations around the CFM wormhole. Actually, Casadio, Fabbri and Mazzacurati [42] obtained two analytical solutions of the spherically

symmetric vacuum brane-world, which are parameterized by the Arnowitt-Deser-Misner (ADM) mass and the PPN parameters. The first solution is given by $g_{tt} = 1 - \frac{2M}{r}$ and $g_{rr} = \frac{r(2r-3M)}{(r-2M)[2r-M(4\beta-1)]}$, where β is a PPN parameter. After a careful analysis, one can find that the PPN parameter β does not affect on the thick accretion disk configurations because the potential W (which determines the equipotential surfaces topology of the disk) does not depend on the metric component g_{rr} . This means that the thick accretion disk configurations are the same as in the usual Schwarzschild black hole spacetime. Therefore, we here only consider the second CFM brane-world solution and study effects of PPN parameter on the configurations of the thick accretion disk.

The paper is organized as follows. In Sec. II, we will briefly review the second CFM brane-world solution [42] and then analyze the changes of the marginally stable orbit and the marginally bound orbit with the PPN parameter for a timelike particle. In Sec. III, we will investigate thick accretion disk configurations around the CFM brane-world compact object and probe effects of the PPN parameter on the disk configurations. Finally, we present a summary.

II. PARTICLE MOTIONS IN THE BACKGROUND OF A COMPACT OBJECT IN THE BRANE-WORLD SCENARIO

Lets us now briefly review the second CFM brane-world solution in [42] and its metric form is

$$ds^2 = - \left(1 - \frac{1}{\gamma} + \frac{1}{\gamma} \sqrt{1 - \frac{2\gamma M}{r}} \right)^2 dt^2 + \left(1 - \frac{2\gamma M}{r} \right)^{-1} dr^2 + r^2 d\theta^2 + r^2 \sin^2 \theta d\phi^2, \quad (1)$$

which is spherically symmetric since it is invariant under a rotation or reflection transformation. The solution is asymptotically flat and owns an ADM mass parameter M and a PPN parameter γ . However, the geometric properties of the spacetime (1) depend on the value of γ . As $\gamma = 1$, it reduces to the usual Schwarzschild black hole spacetime and the event horizon is located at $r = 2M$. As $\gamma > 1$, one can find that the only a singularity in the metric lies at $r = r_0 = 2M\gamma$, where all the curvature invariants are regular. Moreover, $r = r_0$ is a turning point for all physical curves. Thus, the metric (1) describes geometry of a wormhole with a throat radius $r_{\text{throat}} = 2M\gamma$ in this case. As $\gamma < 1$, the metric is singular at r_0 and at the null surface $r = r_s = 2M/(2-\gamma)$. Along this null surface the Ricci scalar R diverges as $R \sim 1/(\sqrt{r-r_0} - \sqrt{r_H-r_0})$. In other words, the metric (1) describes geometry of a naked singularity with a singular null surface $r_s = 2M/(2-\gamma)$. Therefore, the value of γ plays a key role in the global causal structure of the spacetime (1). The analyses of the structure spacetime shows that the solution (1) describes geometry of a pathological naked singularity as $\gamma < 1$, or a black hole as $\gamma = 1$, or a regular wormhole as $\gamma > 1$ [42, 43]. As in [16], in order to visualize the spacetime (1), we present

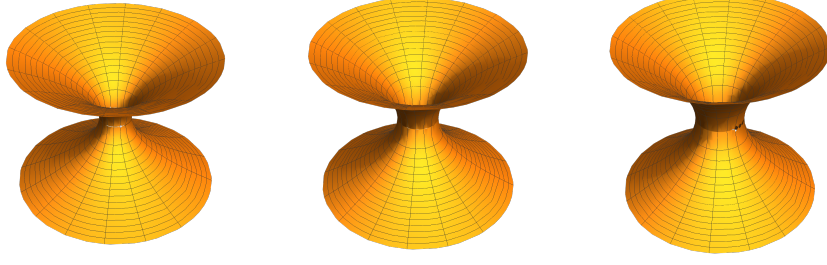


FIG. 1: The embedding diagrams of the metric (1). The left, middle and right panels correspond to the cases $\gamma = 0.8, 1$ and 1.2 , respectively. Here we set $M = 1$.

the embedding diagrams in Fig.1 where the equatorial slice $\theta = \pi/2$ at some fix moment in time $t = \text{constant}$ is embed into three-dimensional Euclidean space $ds^2 = dz^2 + dr^2 + r^2 d\phi^2$ with $dz = \pm \sqrt{r/(r - 2M\gamma) - 1} dr$.

To study the thick accretion disk configurations in the background of a compact object in the brane-world scenario (1), one must get the radius of the marginally stable orbit r_{ms} and the marginally bound orbit r_{mb} for a single timelike particle moving in the spacetime, which are two essential quantities for determining thick disk configurations around a compact object. For the spacetime (1), the Lagrangian density of a single timelike particle's motion

$$\mathcal{L} = \frac{1}{2} g_{\mu\nu}(x) \dot{x}^\mu \dot{x}^\nu, \quad (2)$$

does not contain the time coordinate t and the angular coordinate ϕ , so there are two conserved quantities E and L for the particle, which respectively correspond to its energy and angular momentum. With these conserved quantities, the motion equation of the timelike particle moving in the equatorial plane can be further expressed as

$$\dot{r}^2 - \left(1 - \frac{1}{\gamma} + \frac{1}{\gamma} \sqrt{1 - \frac{2\gamma M}{r}}\right)^{-2} \left(1 - \frac{2\gamma M}{r}\right) \left[E^2 - V_{\text{eff}}(r)\right] = 0, \quad (3)$$

with the effective potential

$$V_{\text{eff}}(r) = \left(\frac{L^2}{r^2} + 1\right) \left(1 - \frac{1}{\gamma} + \frac{1}{\gamma} \sqrt{1 - \frac{2\gamma M}{r}}\right)^2. \quad (4)$$

From the condition of circular orbit $V_{\text{eff}} = E^2$ and $V'_{\text{eff}} = 0$ [21, 44, 45], one can obtain that

$$E^2 = \frac{r - 2\gamma M + (\gamma - 1) \sqrt{r(r - 2\gamma M)}}{r - 3\gamma M + (\gamma - 1) \sqrt{r(r - 2\gamma M)}} \left(1 - \frac{1}{\gamma} + \frac{1}{\gamma} \sqrt{1 - \frac{2\gamma M}{r}}\right)^2, \quad (5)$$

$$L^2 = \frac{\gamma M r^2}{r - 3\gamma M + (\gamma - 1) \sqrt{r(r - 2\gamma M)}}.$$

Combining E and L in Eq.(5) with the condition $V''_{\text{eff}}(r) = 0$, one can find that

$$(\gamma^2 - 2\gamma + 2)r^2 + \gamma(3\gamma^2 - 6\gamma + 11)Mr + 12M^2\gamma^2 + (\gamma - 1)(2r - 9M\gamma)\sqrt{r^2 - 2\gamma Mr} = 0, \quad (6)$$

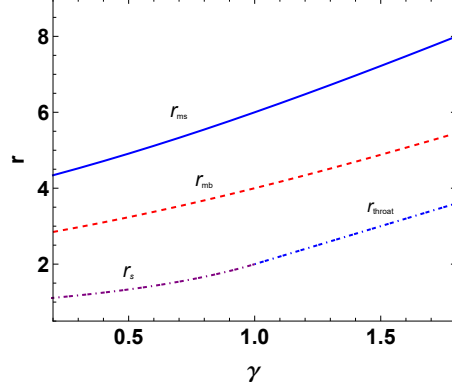


FIG. 2: Changes of the marginally stable orbit radius r_{ms} and the marginally bound orbit radius r_{mb} with the PPN parameter γ . The blue line and the dashed red line denote the radii r_{ms} and r_{mb} , respectively. The purple dot dash line corresponds to the position of the naked singularity r_s and the blue dot dash line is the throat radius r_{throat} . Here we set $M = 1$.

which gives the radius of the marginally stable orbit

$$r_{\text{ms}} = \begin{cases} \frac{M}{6(\gamma-2)} [4(3\gamma^2 - 6\gamma - 4) - (1 + \sqrt{3}i)\mathcal{A}_1\mathcal{B}_1^{-1/3} - (1 - \sqrt{3}i)\mathcal{B}_1^{1/3}], & 0 < \gamma \leq 2, \\ \frac{M}{3(\gamma-2)} [2(3\gamma^2 - 6\gamma - 4) + \mathcal{A}_1\mathcal{B}_1^{-1/3} + \mathcal{B}_1^{1/3}], & \gamma > 2, \end{cases} \quad (7)$$

with

$$\begin{aligned} \mathcal{A}_1 &= 3\gamma(\gamma - 2)(3\gamma^2 - 6\gamma + 19) + 64, \\ \mathcal{B}_1 &= 27\gamma(\gamma - 1)(\gamma - 2)\sqrt{-(9\gamma^4 - 36\gamma^3 + 93\gamma^2 - 114\gamma + 176)} - 27\gamma^6 + 162\gamma^5 - 459\gamma^4 \\ &\quad + 756\gamma^3 - 1224\gamma^2 + 1368\gamma - 512. \end{aligned}$$

The marginally bound orbit r_{mb} is the innermost unstable circular orbit for a timelike particle [21, 44, 45], which can be determined by $V_{\text{eff}} = 1$ and $V'_{\text{eff}} = 0$, i.e.,

$$2(\gamma^2 - 3\gamma + 2)r^2 - \gamma(3\gamma^2 - 12\gamma + 10)Mr + 4M^2\gamma^2 - 2(\gamma - 1)[(\gamma - 2)r + 3M\gamma]\sqrt{r^2 - 2\gamma Mr} = 0. \quad (8)$$

Solving the above equation, we obtain the radius of the marginally bound orbit

$$r_{\text{mb}} = \begin{cases} \frac{M}{12(\gamma-1)(\gamma-2)} [(9\gamma^3 - 24\gamma^2 - 8\gamma + 24) + \mathcal{A}_2\mathcal{B}_2^{-1/3} + \mathcal{B}_2^{1/3}], & 0 < \gamma \leq 0.94026, \quad \text{or} \quad \gamma > 2, \\ \frac{M}{24(\gamma-1)(\gamma-2)} [2(9\gamma^3 - 24\gamma^2 - 8\gamma + 24) - \frac{(1+\sqrt{3}i)\mathcal{A}_2}{\mathcal{B}_2^{1/3}} - (1 - \sqrt{3}i)\mathcal{B}_2^{1/3}], & 0.94026 < \gamma \leq 2, \end{cases} \quad (9)$$

with

$$\begin{aligned} \mathcal{A}_2 &= 81\gamma^6 - 432\gamma^5 + 1008\gamma^4 - 1488\gamma^3 + 1696\gamma^2 - 1248\gamma + 384, \\ \mathcal{B}_2 &= 48(\gamma - 1)^2(9\gamma^3 - 32\gamma^2 + 32\gamma - 8)\sqrt{-3(27\gamma^4 - 54\gamma^3 + 117\gamma^2 - 108\gamma + 20)} + 729\gamma^9 - 5382\gamma^8 \\ &\quad + 21384\gamma^7 - 49464\gamma^6 + 73872\gamma^5 - 57744\gamma^4 - 224\gamma^3 + 39168\gamma^2 - 28800\gamma + 6912. \end{aligned} \quad (10)$$

Fig. 2 shows that both the marginally stable orbit radius r_{ms} and the marginally bound orbit radius r_{mb} increase with the PPN parameter γ of the CFM brane-world compact object. We also present the sizes of

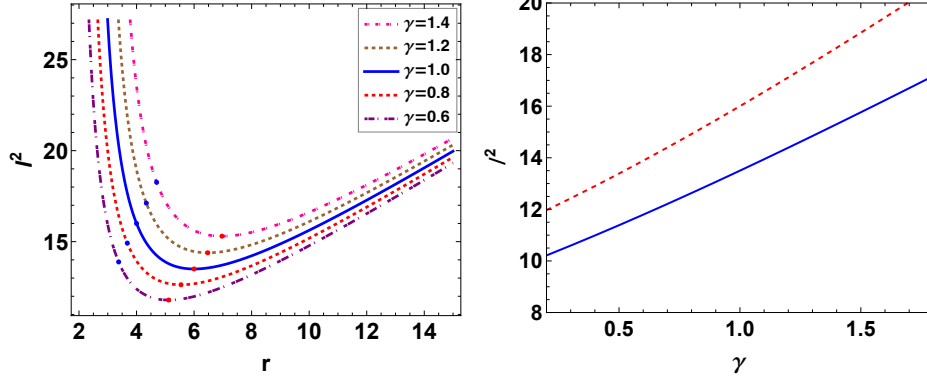


FIG. 3: Changes of the specific angular momentum l^2 with the circular orbit radius r for different PPN parameters γ . In the left panel, the blue and red dots indicate the values of l_{mb}^2 and l_{ms}^2 , respectively. In the right panel, the blue line and the dashed red line correspond the values of l^2 at the marginally stable orbit r_{ms} and the marginally bound orbit r_{mb} , respectively. Here we set $M = 1$.

the singularity r_s and of the throat r_{throat} for different γ , and show that the marginally stable orbit and the marginally bound orbit are outside the naked singularity as $\gamma < 1$ or the wormhole throat as $\gamma > 1$. From Eq.(5), one can find that the specific angular momentum and energy l for the particle moving along the circular orbit with the radius r can be expressed as

$$l^2 \equiv \frac{L^2}{E^2} = \frac{M\gamma^3 r^2}{r - 2\gamma M + (\gamma - 1)\sqrt{r(r - 2\gamma M)}} \left(1 - \frac{1}{\gamma} + \frac{1}{\gamma} \sqrt{1 - \frac{2\gamma M}{r}} \right)^{-2}, \quad (11)$$

Above equations govern the particle motion. From Fig.3, one can find that the specific angular momentum for the particle moving along circular orbit increases with the spacetime parameter γ . Moreover, we also find that $l^2(r_{\text{mb}}) > l^2(r_{\text{ms}})$ for each value of γ .

III. THICK ACCRETION DISK CONFIGURATIONS AROUND THE BRANE-WORLD COMPACT OBJECT

Let us now to study thick accretion disk configurations around the CFM brane-world compact object (1). As in previous works [4–10, 21–26], here we adopt the test-fluid approximation where the accretion flow in the disk is a barotropic perfect fluid with positive pressure and its self-gravity is negligible so that the influence of the disk on the background spacetime is negligible. We also consider that the fluid is axisymmetric and stationary, which means that the physical variables depend on only the coordinated r and θ . Finally, we assume that the rotation of perfect fluid is restricted to be in the azimuthal direction. With these assumptions, the four-velocity and stress-energy tensor of the perfect fluid can be expressed as [46]

$$u^\mu = (u^t, 0, 0, u^\phi), \quad T_{\mu\nu} = (\epsilon + p)u_\mu u_\nu + pg_{\mu\nu}, \quad (12)$$

where ϵ and p are the total energy density and the pressure for a comoving observer, respectively. The corresponding redshift factor in the static spacetime (1) can be is given by

$$u_t = \sqrt{\frac{g_{tt}g_{\phi\phi}}{l^2g_{tt} + g_{\phi\phi}}}, \quad (13)$$

where l is the specific angular momentum. From the conservation for the perfect fluid $\nabla_\nu T^\nu_\mu = 0$, one can obtain [46]

$$\frac{\nabla_\mu p}{\epsilon + p} = -\nabla_\mu \ln(u_t) + \frac{\Omega \nabla_\mu l}{1 - \Omega l}, \quad (14)$$

where $\Omega \equiv u^\phi/u^t$ is the angular velocity of the fluid. The specific angular momentum l depends on the circular orbit radius of the particle motion and the covariant derivative $\nabla_\mu l$ describes the changes of the specific angular momentum l for particles moving along two adjacent circular orbits in the fluid. For a barotropic fluid, ϵ is a function of p , so the the right-hand side of (14) becomes a differential. This implies that either $dl = 0$ or $\Omega = \Omega(l)$. This result is known as the (relativistic) von Zeipel theorem. For a barotropic fluid, one can get a solution of the above equation by integration, i.e.,

$$\int_{p_{\text{in}}}^p \frac{dp}{\epsilon + p} = -\ln \frac{|u_t|}{|(u_t)_{\text{in}}|} + \int_{l_{\text{in}}}^l \frac{\Omega dl}{1 - \Omega l} = W_{\text{in}} - W. \quad (15)$$

The subscript ‘‘in’’ denotes that the quantity is evaluated at at the inner edge of the disk. The potential W determines the topologies of equipotential surfaces in the disk. Therefore, once the expression $\Omega = \Omega(l)$ is given, one can obtain the equipotential surfaces in the disk. Although in the real astrophysical situations, l would be given by certain dissipative processes with timescales much longer than the dynamical timescale, such as the possible viscosity. It must be pointed out that the viscosity in astrophysical accretion disks can not come from ordinary molecular viscosity since such ordinary viscosity are too weak to explain observed phenomena. Up to now, these dissipative processes are not yet fully understood. A possible alternative way of prescribing this unknown dissipative processes is to directly set the angular momentum l in the model as a constant [46] or a non-constant angular momentum distribution [47, 48]. Here, we adopt the model with the constant distribution of angular momentum $l = l_0$ to study the equilibrium configurations in the thick disk for different parameters in the CFM brane-world compact object (1). In this model, the potential W can be further simplified as

$$W = -\ln |u_t|. \quad (16)$$

The thick disk configurations depend heavily on the specific angular momentum l_0 . From Fig.3, one can obtain that there is a minimum l_{ms} for the specific angular momentum l_0 , so the fluid with $l_0 < l_{\text{ms}}$ can not

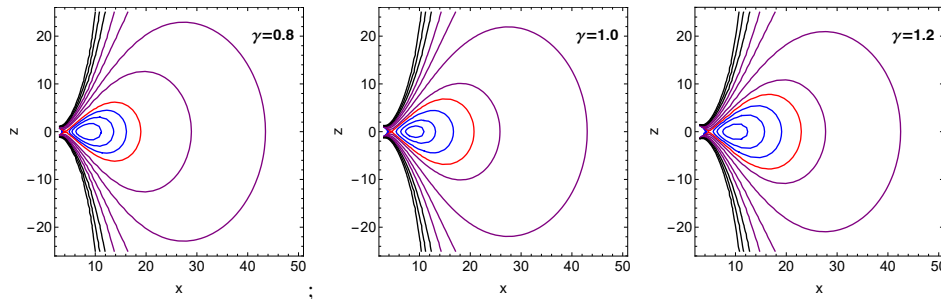


FIG. 4: Equipotential surfaces for different choices of γ and constant $l_0 = (l_{\text{mb}} + l_{\text{ms}})/2$. The red line indicates the torus with a cusp corresponding to the maximum of W on the equatorial plane. Blue lines indicate closed tori, purple lines bound structures without inner edge, and black lines open surfaces.

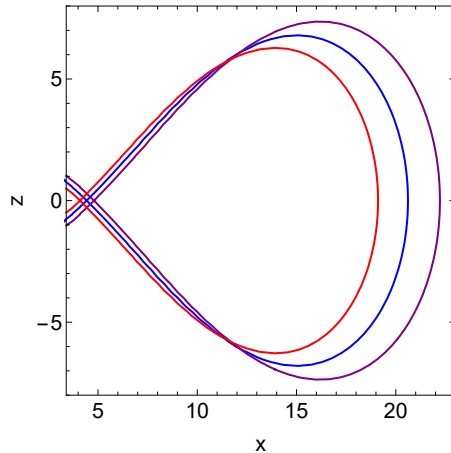


FIG. 5: Equipotential surfaces corresponded to Roche lobe for different choices of γ and constant $l_0 = (l_{\text{mb}} + l_{\text{ms}})/2$. The red, blue and purple lines denote the cases with $\gamma = 0.8, 1.0$ and 1.2 , respectively.

move along a circular orbit and it is no possible to exist a disk around a CFM brane-world compact object in this case. When $l_0 = l_{\text{ms}}$, there exists only a ring around the compact object. As $l_{\text{ms}} < l_0 < l_{\text{mb}}$, it is found to exist bound disk structures with a cusp. As l_0 increases to $l_0 = l_{\text{mb}}$, one can find that the cusp is located at the marginally closed surface that just extents to infinity [21–26]. As l_0 further increases to $l_0 > l_{\text{mb}}$, one can find that the disk still exists but not cusp.

To probe the dependence of the disk configurations on the spacetime parameter γ , we set $l_0 = \frac{1}{2}(l_{\text{ms}} + l_{\text{mb}})$, and ensure $l_{\text{ms}} < l_0 < l_{\text{mb}}$. Combining Eqs.(1) with (13) and (16), one can obtain the potential function W and probe the properties of the corresponding equipotential surfaces for different γ . Fig. 4 shows the disk configurations around a CFM brane-world compact object (1). In each panel, the blue lines denote possible bound disk structures in which there are no actual accretion and the fluid rotate only around the compact object. The red line corresponds to the equipotential surface with a cusp located at the marginally closed surface, which plays the same role as a Roche lobe and the matter from a disk outside this surface would flow over the cusp and accrete into the central compact object. The purple lines denote bound structures

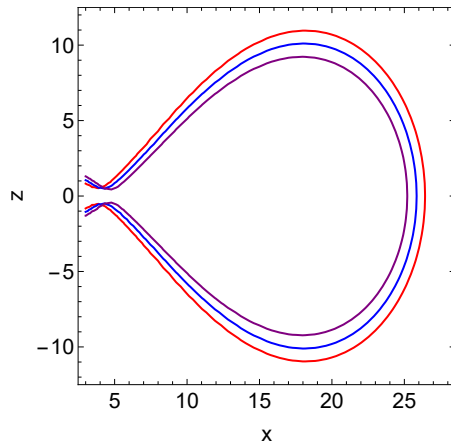


FIG. 6: Equipotential surfaces with $W = -0.01$ outside the Roche lobe for different choices of γ and constant $l_0 = (l_{\text{mb}} + l_{\text{ms}})/2$. The red, blue and purple lines denote the cases with $\gamma = 0.8, 1.0$ and 1.2 , respectively.

without inner edge but with a marginally outer edge, and black lines denote the cases with open surfaces. The closed equipotential surface at infinite distance satisfies $W = 0$. With the increase of the parameter γ , we find that the value W of the equipotential surface corresponded to the Roche lobe increases, and the surface of the Roche lobe gradually moves away from the central wormhole. The latter can be explained by a fact that both the marginally stable orbit radius r_{ms} and the marginally bound orbit radius r_{mb} increase with the parameter γ of the brane-world compact object (1). Moreover, with the increase of γ , the thickness of the region enclosed by the Roche lobe decreases near the compact object and increases for the region far from the compact object, but the area of the total region enclosed by the Roche lobe increases as shown in Fig. 5, which means that the region of existing bound disk structures without accretion increases with the γ . From Fig. 5, we also find that the cusp is the point nearest the centre of the compact object in the Roche lobe. In the table (I), we compare the radial coordinate of this cusp r_{cusp} with the size of the compact object and find that the Roche lobe is outside the compact object. Fig. 6 presents the equipotential surface with $W = -0.01$

γ	0.8	1.0	1.2
r_{cusp}	4.082	4.437	4.809
r_{s}	1.667	–	–
r_{H}	–	2.0	–
r_{throat}	–	–	2.4

TABLE I: Comparison between the cusp (the nearest point to the centre of the compact object in the Roche lobe) and the size of the compact object for different γ .

outside the Roche lobe for different γ , where the matter filling in this region can be accreted into the central compact object. It is illustrated that the size of accretion disk decreases with the PPN parameter of the CFM brane-world compact object, which means that the size of accretion disk for the CFM brane-world wormhole

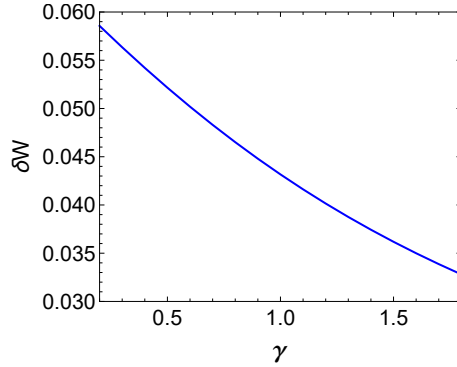


FIG. 7: Change of δW with the PPN parameter γ for the brane-world compact object (1) in the case $l_0 = l_{\text{mb}}$.

is less than that for the CFM brane-world naked singularity.

The pressure gradient in the thick disk is very important for the fluid to keep balance with gravitational and centrifugal forces [22–26]. Since the pressure gradient is related to the difference δW between different equipotential surfaces, we plot the maximal difference δW between the potential values at the cusp and the center of the disk. Fig. 7 illustrates that the difference δW and the pressure gradient in the equilibrium thick torus decrease with the PPN parameter γ for the CFM brane-world compact object (1). It is also shown that the pressure gradient in the disk is larger in the CFM brane-world naked singularity, and is smaller in the CFM brane-world wormhole case. These results could help to further understand compact objects in the brane-world.

IV. SUMMARY

We have studied the equipotential surfaces in the thick accretion disk around the CFM brane-world compact object with a PPN parameter. It is shown that with the increase of the PPN parameter, the size for the thick accretion disk decreases, but the Roche lobe increases. This implies that the larger PPN parameter results in the larger region of existing bound disk structures in which the fluid is not accreted into the central wormhole. Moreover, with the increase of the parameter γ , the surface of the Roche lobe increases, and the Roche lobe gradually moves away from the central compact object. This can be explained by a fact that both the marginally stable orbit radius r_{ms} and the marginally bound orbit radius r_{mb} increase with the parameter γ . In addition, the thickness of the region enclosed by the Roche lobe decreases with the parameter γ near the compact object, but increases in the region far from the compact object. Finally, we have also studied the difference δW between the potential values at the cusp and the center of the disk, which shows that the

pressure gradient in the equilibrium thick torus the CFM brane-world compact object (1) decreases with the parameter γ . Thus, the pressure gradient in the disk in the background of the CFM brane-world compact object is larger than that in the Schwarzschild background as $\gamma < 1$, but is smaller as $\gamma > 1$. These results could help to understand the CFM brane-world compact object and its thick accretion disk.

V. ACKNOWLEDGMENTS

This work was supported by the National Natural Science Foundation of China under Grant No.12275078, 11875026, 12035005, and 2020YFC2201400.

-
- [1] Shakura N I and Sunyaev R A. Black holes in binary systems. Observational appearance. *A&A*, 24:337–355, 1973.
 - [2] Igumenshchev I V, Abramowicz M A, and Novikov I D. Slim accretion discs: a model for ADAF-SLE transitions. *Mon. Not. Roy. Astron. Soc.*, 298(4):1069–1078, 1998.
 - [3] Szuszkiewicz E. Slim accretion discs with different viscosity prescriptions. *Mon. Not. Roy. Astron. Soc.*, 244:377–383, 1990.
 - [4] Eardley D M, Lightman A P, and Shapiro S L. Cygnus X-1: a two-temperature accretion disk model which explains the observed hard X-ray spectrum. *Astrophys. J. Lett.*, 199:L153–L155, 1975.
 - [5] Narayan R and Yi I. Advection-dominated Accretion: Underfed Black Holes and Neutron Stars. *Astrophys. J.*, 452:710, 1995.
 - [6] Turolla R and Dullemond C P. Advection-dominated inflow/outflows from evaporating accretion disks. *Astrophys. J.*, 531(1):L49, 2000.
 - [7] Shane W D, Chris D, and Omer M B. Testing accretion disk theory in black hole x -ray binaries. *Astrophys. J.*, 647(1):525, 2006.
 - [8] Ichimaru S. Bimodal behavior of accretion disks: theory and application to Cygnus X-1 transitions. *Astrophys. J.*, 214:840–855, 1977.
 - [9] Font J A and Daigne F. The runaway instability of thick discs around black holes - I. The constant angular momentum case. *Mon. Not. Roy. Astron. Soc.*, 334(2):383–400, 2002.
 - [10] Paczynski B and Abramowicz M A. A model of a thick disk with equatorial accretion. *Astrophys. J.*, 253:897–907, 1982.
 - [11] Montesinos M. Review: Accretion Disk Theory. *arXiv: 1203.6851*, 2012.
 - [12] Abramowicz M A and Fragile P C. Foundations of black hole accretion disk theory. *Living reviews in relativity*, 16(1):1, 2013.
 - [13] Liu B F and Qiao E. Accretion around black holes: The geometry and spectra. *arXiv: 2201.06198*.
 - [14] Bahamonde S and Jamil M. Accretion Processes for General Spherically Symmetric Compact Objects. *Eur. Phys. J. C*, 75:508, 2015.
 - [15] Ahmed A K, Azreg-Aïnou M, Faizal M, and Jamil M. Cyclic and heteroclinic flows near general static spherically symmetric black holes. *Eur. Phys. J. C*, 76(5):280, 2016.
 - [16] Jusufi K, Kumar S, Azreg-Aïnou M, Jamil M, Wu Q, and Bambi C. Constraining wormhole geometries using the orbit of S2 star and the Event Horizon Telescope. *Eur. Phys. J. C*, 82(7):633, 2022.
 - [17] Chen S, Jing J, Qian W L, and Wang B. Black hole images: A review. *Sci. China Phys. Mech. Astron.*, 66(6):260401, 2023.
 - [18] Liu X, Chen S, and Jing J. Polarization distribution in the image of a synchrotron emitting ring around a regular black hole. *Sci. China Phys. Mech. Astron.*, 65(12):120411, 2022.
 - [19] Zhou X, Chen S, and Jing J. Effect of noncircularity on the dynamic behaviors of particles in a disformal rotating black-hole spacetime. *Sci. China Phys. Mech. Astron.*, 65(5):250411, 2022.
 - [20] Bahamonde S, Golovnev A, Guzmán M, Said J L, and Pfeifer C. Black holes in f(T,B) gravity: exact and perturbed solutions. *JCAP*, 01(01):037, 2022.
 - [21] Bahamonde S, Faraji S, Hackmann E, and Pfeifer C. Thick accretion disk configurations in the Born-Infeld teleparallel gravity. *Phys. Rev. D*, 106(8):084046, 2022.
 - [22] Cassing M and Rezzolla L. Equilibrium non-selfgravitating tori around black holes in parameterised spherically symmetric spacetimes. *arXiv:2302.09135*.
 - [23] Gimeno-Soler S, Font J, Herdeiro C, and Radu E. Magnetized accretion disks around Kerr black holes with scalar hair: Constant angular momentum disks. *Phys. Rev. D*, 99(4):043002, 2019.

- [24] Gimeno-Soler S, Font J, Herdeiro C, and Radu E. Magnetized accretion disks around Kerr black holes with scalar hair: Nonconstant angular momentum disks. *Phys. Rev. D*, 104(10):103008, 2021.
- [25] Cruz-Orsorio A, Gimeno-Soler S, Font J A, De Laurentis M, and Mendoza S. Magnetized discs and photon rings around Yukawa-like black holes. *Phys. Rev. D*, 103(12):124009, 2021.
- [26] Gimeno-Soler S, Pimentel O M, Lora-Clavijo F D, Cruz-Orsorio A, and Font J A. Magnetised tori with magnetic polarisation around Kerr black holes: variable angular momentum discs. *arXiv: 2303.15867*.
- [27] Randall L and Sundrum R. Large mass hierarchy from a small extra dimension. *Phys. Rev. Lett.*, 83:3370–3373, 1999.
- [28] Randall L and Sundrum R. An alternative to compactification. *Phys. Rev. Lett.*, 83:4690–4693, 1999.
- [29] Dadhich N, Maartens R, Papadopoulos P, and Rezzani V. Black holes on the brane. *Phys. Lett. B*, 487:1–6, 2000.
- [30] Germani C and Maartens R. Stars in the brane world. *Phys. Rev. D*, 64:124010, 2001.
- [31] Ponce de Leon J. Static exteriors for nonstatic braneworld stars. *Class. Quantum Grav.*, 25(7):075012, 2008.
- [32] Molina C, Pavan A B, and Medina Torrejón T E. Electromagnetic perturbations in new brane world scenarios. *Phys. Rev. D*, 93(12):124068, 2016.
- [33] Heydari-Fard M, Razmi H, and Sepangi H R. Brane-world black hole solutions via a confining potential. *Phys. Rev. D*, 76(6):066002, 2007.
- [34] Randall L and Sundrum R. Large Mass Hierarchy from a Small Extra Dimension. *Phys. Rev. Lett.*, 83(17):3370–3373, 1999.
- [35] Lin C M. On the nature of cosmic strings in the brane world. *arXiv: 2208.09589*, page arXiv:2208.09589, 2022.
- [36] Tadros P and Assaad Abdel-Raouf M. Eliminating black holes singularity in Brane world Cosmology. *arXiv e-prints: 2203.15785*.
- [37] Harko T and Mak M K. Vacuum solutions of the gravitational field equations in the brane world model. *Phys. Rev. D*, 69:064020, 2004.
- [38] Mak M K and Harko T. Can the galactic rotation curves be explained in brane world models? *Phys. Rev. D*, 70:024010, 2004.
- [39] Harko T and Mak M K. Conformally symmetric vacuum solutions of the gravitational field equations in the brane-world models. *Annals of Physics*, 319(2):471–492, 2005.
- [40] Harko. 636(1):8, 2006.
- [41] Pun C S J, Kovács Z, and Harko T. Thin accretion disks onto brane world black holes. *Phys. Rev. D*, 78:084015, 2008.
- [42] Casadio R, Fabbri A, and Mazzacurati L. New black holes in the brane world? *Phys. Rev. D*, 65:084040, 2002.
- [43] Tan H S. Tidal Love Numbers of Braneworld Black Holes and Wormholes. *Phys. Rev. D*, 102(4):044061, 2020.
- [44] Berry T, Simpson A, and Visser M. Photon spheres, iscos, and oscos: Astrophysical observables for regular black holes with asymptotically minkowski cores. *Universe*, 7(1), 2021.
- [45] Song Y. The evolutions of the innermost stable circular orbits in dynamical spacetimes. *Eur. Phys. J. C*, 81(10):875, 2021.
- [46] Abramowicz M, Jaroszynski M, and Sikora M. Relativistic, accreting disks. *A&A*, 63:221–224, 1978.
- [47] Lei Q, Abramowicz M A, Fragile P C, Horak J, Machida M, and Straub O. The Polish doughnuts revisited I. The angular momentum distribution and equipressure surfaces. *Astron. Astrophys.*, 498:471–477, 2009.
- [48] Wielgus M, Fragile P C, Wang Z, and Wilson J. Local Stability of Strongly Magnetized Black Hole Tori. *Mon. Not. Roy. Astron. Soc.*, 447:3593, 2015.